Pediatric RESEARCH

www.nature.com/pr

CLINICAL RESEARCH ARTICLE

Pulmonary arteries of Williams syndrome patients exhibit altered serotonin metabolism genes and degenerated medial layer architecture

Xiaoyuan Ma[1], R. Thomas Collins[2], Ariana Goodman[1], Frank L. Hanley[1] and Robert Kirk Riemer[1]

BACKGROUND: Williams–Beuren syndrome (WS) is characterized by cardiovascular abnormalities associated with a multigene deletion on 7q11.23, in particular elastin (ELN). Peripheral pulmonary artery stenosis (PPAS) frequently affects pediatric patients with WS. Molecular investigation of WS pulmonary arterial (PA) tissue is limited by tissue scarcity.
METHODS: We compared transcriptomes, tissue architecture, and localized changes in protein expression in PA tissue from patients with WS ($n = 8$) and donors ($n = 5$).
RESULTS: Over 100 genes were differentially expressed at the ≥4-fold level, including genes related to the serotonin signaling pathway: >60-fold downregulation of serotonin transporter SLC6A4 and >3-fold upregulation of serotonin receptor HTR2A. Histologic examination revealed abnormal elastin distribution and smooth muscle cell morphology in WS PA, with markedly shorter, disorganized elastin fibers, and expanded proteoglycan-rich extracellular matrix between muscle layers.
CONCLUSIONS: There were significant abnormalities in the PA expression of genes regulating serotonin signaling, metabolism, and receptors in WS. Those changes were associated with distinct changes in the arterial structure and may play a role in the stenosis-promoting effects of elevated shear stress at PA bifurcations in WS.

Pediatric Research (2021) 90:1065–1072; https://doi.org/10.1038/s41390-020-01359-5

IMPACT:

- Serotonin pathway signaling is significantly altered in the pulmonary arteries of patients with Williams syndrome and severe peripheral arterial stenosis.
- The present study compares the histological and biochemical characteristics of pulmonary arteries from patients with Williams syndrome to those of controls, something that has not, to our knowledge, been done previously. It demonstrates marked abnormalities in the pulmonary arteries of patients with Williams syndrome, especially significant pathologic alterations in the signaling of the serotonin pathway.
- The findings of this study provide direction for the development of potential therapies to treat pulmonary artery stenosis in patients with Williams syndrome.

INTRODUCTION

Williams–Beuren syndrome (WS), an inherited disorder associated with an ~1.7-Mb deletion on chromosome 7q11.23, is characterized by phenotypic abnormalities in the cardiovascular, connective tissue, and central nervous systems.[1] Cardiovascular abnormalities occur in approximately 80% of patients with WS.[2] The majority of those lesions are related to generalized arteriopathy[3,4] presenting as arterial stenoses primarily of large- and medium-sized vessels, with supravalvar aortic stenosis (SVAS) and peripheral pulmonary artery stenosis (PPAS) being the most common.[5–8] PPAS usually manifests clinically in early childhood and requires interventions in up to a third of cases.[9] Examination of the arteries reveals a normal intimal layer with symmetrical narrowing of the lumen of extrapulmonary branches characterized by tunica media hypercellularity.[8]

Elastin plays a fundamental role in the molecular and biomechanical mechanisms in WS. Hemizygosity of *ELN*, the gene encoding elastin, results in vascular smooth muscle cell (SMC) hyperplasia of the tunica media and arterial stenosis similar to that seen in WS.[10] Elastin bound to other extracellular matrix (ECM) proteins form "contractile units," serving a critical role in both structural integrity and the homeostatic sensing of mechanical wall stress.[6] Further, elastin fibril binding to SMCs via the elastin-binding protein on the SMC surface is believed to be a key regulatory signal governing SMC density during vascular wall development.[11] Mochizuki et al. have suggested that elastin degradation products or abnormally formed elastin fibrils binding to the elastin-binding protein on the SMC surface disrupts the normal negative feedback mechanism through which elastin limits SMC proliferation, thus potentially resulting in abnormal tunica media layer organization

[1]Congenital Cardiac Division, Department of Cardiothoracic Surgery, Stanford University, CA, Stanford, USA and [2]Department of Pediatrics - Cardiology, Stanford University, CA, Stanford, USA
Correspondence: Robert Kirk Riemer (riemerk@stanford.edu)

Received: 21 August 2020 Revised: 16 December 2020 Accepted: 18 December 2020
Published online: 2 February 2021

Table 1. Study patient demographics.

Patient	Specimen	Age	Sex	Diagnosis	Analyses conducted
#98	PA	6	M	WS, SVAS, PPAS	MA
#594	PA	8	M	WS, SVAS, PPAS	MA
#605	PA	22	M	WS, PPAS	MA
#662	PA	43	F	WS, PPAS	MA, IHC
#686	PA	12	F	WS, SVAS, PPAS	MA, IHC
#720	PA	20	M	WS, PPAS	MA, IHC
#770	PA	27	F	WS, PPAS	IHC
#792	PA	12	M	WS, PPAS	IHC
#258	PA	8	F	Donor	MA, IHC
#361	PA	18	F	Donor	IHC
#380	PA	12	F	Donor	MA
#523	PA	36	M	Donor	MA, IHC
#611	PA	12	M	Donor	MA, IHC

Age in months.
F female, *M* male, *PA* pulmonary artery, *SVAS* supravalvular aortic stenosis, *PPAS* peripheral pulmonary artery stenosis, *MA* HTA 2.0 transcriptome microarray, *IHC* immunohistochemistry.

through SMC proliferation. Further, tropoelastin, the immature precursor to mature elastin fibrils, may contribute to activation of the normally non-proliferative SMC population, leading to occlusive vascular pathologies, such as those in WS.

In spite of the vital role of elastin in the arterial pathology in WS, studies in Eln+/− mice incompletely replicate that pathology.[3] A recent exome-wide analysis demonstrated that the severity of the arterial pathology in patients with WS correlated best with genes other than *ELN*.[12] Further, though all patients with WS have hemizygosity of *ELN*, only about 40% have PPAS,[13] indicating that there is more to the underlying pathology than previously realized. Additionally, PPAS is seen in other populations, such as those with Alagille syndrome where hemizygosity of *ELN* is not present.[14] Given the deficit in our understanding of the underlying mechanisms of PPAS in WS, we sought to analyze the histological, biochemical, and genetic regulatory profiles in pulmonary artery (PA) samples from patients with WS and compared them to donor controls.

METHODS

Patient demographics and specimen collection

For this study, following approval by the Stanford University Institutional Review Board, we obtained tissue samples from patients at Lucile Packard Children's Hospital Stanford. We analyzed conduit PA specimens from two groups of pediatric patients (Table 1): those with WS undergoing surgical correction of PPAS and those whose hearts had been explanted as heart transplant donors (donor group). Specimens were collected in the operating room and transported to the laboratory in cold, buffered saline immersed in ice, and portions were immediately fixed in buffered formalin or flash-frozen in liquid nitrogen and stored at −80 °C.

RNA isolation and transcriptome array

Collected samples were processed for total RNA extraction from 20 to 30 mg of fresh frozen tissue using the TRIzol reagent (Thermo Fisher, CA). RNA samples were further purified using the RNeasy Mini Kit (Qiagen, Redwood City, CA) according to the manufacturer's instructions. Quality of RNA was assessed by ultraviolet absorption spectrophotometry (NanoDrop Technologies, ThermoFisher, Santa Clara, CA) and on-chip electrophoretic separation with quantitation (Bioanalyzer 2100; Agilent Technologies, Santa Clara, CA). Only RNA preparations with an RNA integrity number >7 were used for microarray analysis.

Transcriptome array and data analysis

Intact total RNA from each sample was used for amplification, labeling, and hybridization using the GeneChip WT Plus Reagent Kit according to the manufacturer's instructions (Affymetrix, Santa Clara, CA). Samples were hybridized on Human Transcriptome Array 2.0 slides (Affymetrix) using standard protocols for cRNA labeling, hybridization, and detection procedures as previously described.[15]

Transcriptome Analysis Console (TAC 4.0; Affymetrix, Santa Clara, CA) and Partek Genomic Suite (version 7.0; St Louis, MO) were used to analyze the microarray data. The robust multi-array average algorithm was used for gene- and exon-level intensity analyses. Data were filtered to consider only those probe sets included in the "Core Meta-Probeset." Analysis of variance (ANOVA) and multi-test correction for *p* values were used to identify differentially expressed genes and exons. ANOVA *p* values were corrected using Bonferroni method. Lists of genes and exons with significant variation of the expression levels were generated by using a 0.01 False Discovery Rate as significance level cutoff criterion. To define and identify patterns of gene expression profiles, unsupervised hierarchical clustering analysis was performed based on the values of the differentially expressed genes to determine the relatedness of expression patterns among the sample group. The resulting list of differentially expressed transcripts was uploaded into Ingenuity Pathway Analysis (Ingenuity Systems, Redwood City, CA) as the starting points for gene ontogeny analysis and generation of biological networks. Protein–protein interactions for the selected groups of differentially expressed genes were mapped using the String.org database toolset (String.org), which uses protein sequence information and Gene Ontology (GO) to illustrate interactions (known, actual, and predicted).

Histology

Dissected vessel specimens were fixed in 10% buffered formalin (Fisher Scientific, Fair Lawn, NJ) for 24 h and then embedded in paraffin. Serial PA cross-sections (5 µm) were prepared for analysis. Russell–Movat Pentachrome stain ("Movat," American MasterTech Scientific Inc., Lodi, CA) was used to visualize the presence and distribution of elastic lamina and other components of the ECM (stains elastic fibers, black; proteoglycans, blue; collagen, yellow; fibrinoid mucins; muscle and nuclei, red).

Immunohistochemical analysis

The vessel tissue sections were deparaffinized and rehydrated with phosphate-buffered saline (PBS) by immersion in a descending ethanol series for immunostaining as previously described.[15] Endogenous peroxidase activity was blocked with 1% H_2O_2. Antigen retrieval was performed using 10 mM sodium citrate buffer (pH 6.0) at 90–100 °C for 10 min to unmask the antigenic epitopes, and the staining container was placed at room temperature to cool down for 30 min. The sections then were subjected to three 10-min washes in PBS, covered with a blocking buffer (10% blocking serum in PBS), and incubated for 1 h in a humidified chamber at room temperature. The primary antibodies to HTR1A, HTR2A, and Elastin (Abcam, MA); SLC6A4 (Bioss, MA); and Smooth Muscle Actin (SMA; Dako/Agilent, CA) were prepared according to the respective vendor's instructions and applied to the sections, and the sections were incubated overnight at 4 °C. On the second day, the sections were subjected to three 10-min washes in PBS, and slides were processed for immunoperoxidase detection using either diaminobenzidine (DAB) chromogen (ABC Vectastain system, Vector Laboratories) or fluorescent conjugated Alexa Fluor (green 488; red 595; both from Invitrogen). Negative control slides used exclusion of primary or secondary antibody. After the DAB reaction, sections were washed extensively in PBS and counterstained with hematoxylin (Fisher Scientific) or

fluorescent Hoechst 33342 nuclear stains (Molecular Probes, Invitrogen) before microscopic examination. Fluorescent images were captured with a Nuance Multispectral Imaging System (CRI Inc., Cambridge, MA).

RESULTS

Characteristics of the study groups are reported in Table 1. There were 8 patients (63% male) with WS (median age 16 months, range 6–43 months) and 5 age-matched donors (60% female; median age 12 months, range 8–36 months).

Transcriptomal differences between PA samples from WS and donors

Hierarchical clustering analysis of the regulated genes was performed to assess objectively statistical heterogeneity in expression pattern among groups. The expression magnitude hierarchical clustering heat map (Fig. 1a) demonstrates that >1000 PA genes are differentially expressed (fold change >2.0, $p < 0.05$) in WS PA compared with donor PA. Pairwise analysis identified 1457 differentially regulated genes (Mapped IDs, 814; Unmapped IDs, 643) in WS PA. Quantitation of upregulated and downregulated genes stratified by fold-change cutoff (Fig. 1b) demonstrates that the majority of WS PA genes are downregulated compared with donor PA. In Table 2, we list the 10 most upregulated and downregulated genes. Among the most upregulated genes were cytokines and matrix-remodeling genes.

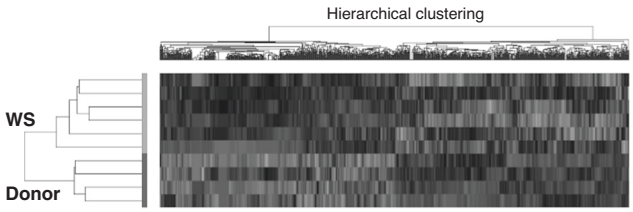

	WS/donor	Activated	Inhibited
Fold >2, p<0.05	814	306	508
Fold >4, p<0.05	151	57	94
Fold >10, p<0.05	32	8	24

Fig. 1 Intensity map of gene expression comparing WS PA vs donor PA. a Heat map array shows the results of pairwise hierarchical clustering analysis of gene transcripts. The dendrogram at the left indicates statistical groupings. The red bars indicate relatively increased expression, and green bars indicate relatively decreased expression, with intermediate intensities indicated by black. **b** Results are tabulated by fold-change cutoff. A total of 367 transcripts were regulated (WS PA, $n = 6$, donor PA, $n = 4$) more than twofold difference cutoff, $p < 0.05$.

Table 2. The 10 most upregulated and downregulated genes in WS pulmonary artery.

Fold change	Gene symbol	Description	p value
319	CYTL1	Cytokine like 1	3.34E−06
27.7	MXRA5	Matrix remodeling associated 5	5.00E−04
19.7	FRZB	Frizzled related protein	1.06E−05
18.4	STC1	Stanniocalcin 1	3.80E−03
15.9	HAPLN1	Hyaluronan and proteoglycan link protein 1	2.41E−05
12.1	PTN	Pleiotrophin	1.00E−04
9.3	FMOD	Fibromodulin	1.40E−03
8.9	CPNE4	Copine 4	6.61E−10
8.6	EDIL3	EGF-like repeats and discoidin domains 3	1.41E−02
8.5	MYO1D	Myosin ID	1.60E−03
−12.8	S100A9	S100 calcium-binding protein A9	1.10E−03
−13.2	ABCA6	ATP-binding cassette subfamily A member 6	6.40E−03
−15.9	APOD	Apolipoprotein D	4.20E−03
−15.9	IF130	IFI30, lysosomal thiol reductase	1.50E−03
−18.4	SCUBE3	Signal peptide, CUB domain, and EGF-like domain containing 3	1.80E−03
−21	SCN7A	Sodium voltage-gated channel alpha subunit 7	4.64E−02
−22.9	C3	Complement C3	3.00E−04
−28.7	VNN2	Vanin 2	1.82E−02
−29.5	CD163	CD163 molecule	1.64E−05
−61	SLC6A4	Solute carrier family 6 member 4 (SERT)	8.33E−05

Fold change is the ratio of gene expression in WS PA compared with control PA (WS/Control). Negative fold change indicates downregulated in WS vs Ctrl.

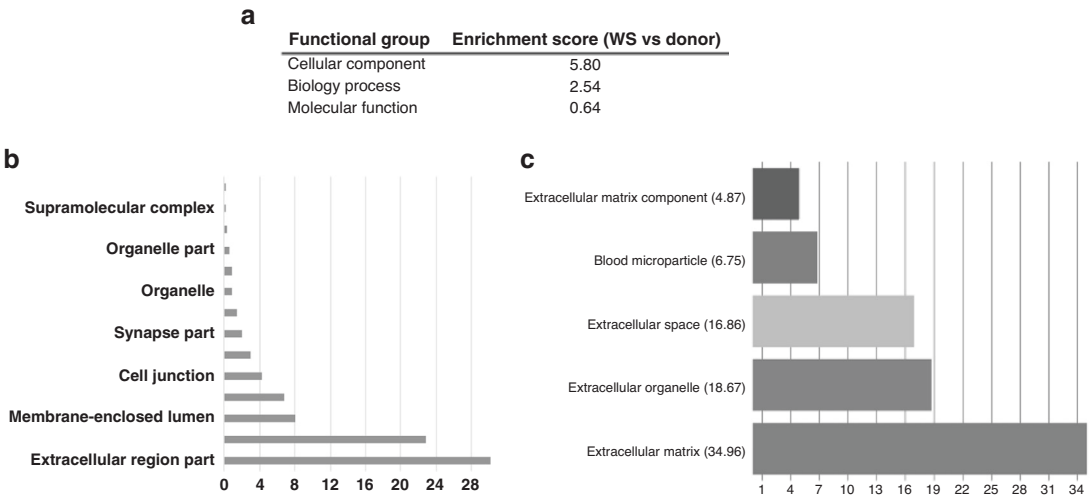

Fig. 2 Functional Gene Ontology classification of the WS regulated genes. a Proportion of significant Gene Ontology (GO) functional groups enriched for the differentially regulated genes in WS relative to donor PA. **b** Major enriched GO class members of the cellular component. **c** Details of the most changed members of the extracellular region functional group. Numbers in parentheses indicate the percentage of genes within the functional group that are differentially regulated in WS.

The gene most downregulated was *SLC6A4*, the serotonin transporter (also referred to as SERT), with >60-fold reduced expression in WS PA. A list of the top 100 most differentially expressed genes in WS PA are provided in Supplemental Table S1.

GO analysis quantified the representation of genes among three functional classifications: Molecular Function, Biological Process, and Cellular Components, as shown in Fig. 2. In WS PA, the Cellular Component was the largest functional group based on GO enrichment score, while Molecular Function had the lowest GO representation. Further, the most significantly represented GO category in the Cellular Components group was the extracellular region, with >35% of ECM genes regulated and ECM component genes most upregulated.

Ingenuity Pathway Analysis provided functional analysis of the canonical gene regulation pathways and major pathway relationships of genes regulated >2-fold. The major canonical pathway exhibiting inhibition status was the serotonin degradation pathway, with 9 molecules associated, including monoamine oxidase (MAO) isoform A that preferentially metabolizes serotonin and generates both ammonia and hydrogen peroxide (Supplemental Fig. S1). Among upstream regulation pathways driving the observed changes in gene expression, the five most represented pathways were *TNF*, *TGFb1*, *INFG*, *IL4*, and *IL10RA* (Table 3). Notably, differences in WS PA genes tended to be in inhibited states (i.e., downregulated), and only transmembrane receptor *IL10RA* pathway was predicted to be in an activated state.

Table 3. Top upstream analysis-predicted activation state in differentially regulated genes.

Upstream regulator	Molecule type	Predicted state	*p* Value of overlap	*z*-Score
TNF	Cytokine	Mixed	1.40E-30	−0.723
TGFB1	Growth factor	Mixed	1.29E-25	−1.326
IFNG	Cytokine	Inhibited	1.01E-22	**−2.989**
IL4	Cytokine	Inhibited	1.91E-17	**−2.804**
IL10RA	Transmembrane receptor	Activated	1.07E-12	2.363

z-Score values in bold type indicate significance level of $p < 0.05$.

Differential expression of genes on 7q11.23 in WS PA

Analysis of expression levels of the 27 genes typically deleted in WS, including *ELN* (Fig. 3), demonstrated that 12 genes (45%) showed very low expression levels (log2 intensity <6), with most of the other genes showing a downregulated trend (i.e., WS intensity lower than donor). Five of these genes (*BAZ1B*, *BCL7B*, *WBSCR22*, *EIF4H*, and *NCF1*) were downregulated >2.0-fold compared with donor PA, and most of these regulated genes encode transcriptional regulatory proteins. The most highly expressed gene in the WS region was *ELN*, and it was expressed at a similar level in both WS and controls.

Differential expression of non-7q11.23 genes in WS PA

Many changed genes affecting mechanical force sensing in the vascular wall are not in the WS deleted region. We observed the reciprocal regulation of two Wnt pathway soluble receptor/binding protein genes: Frizzled (*FRZB*), upregulated ~20-fold and Secreted Frizzled-related protein (*SFRP*) was downregulated ~4-fold. Expression of *IGFBP* was down 3-fold; *ADAMTS5* expression was down 4-fold; and *HAPLN1* expression was markedly upregulated (12-fold).

Serotonin pathway-related gene expression

As shown in Table 4, one of the most downregulated genes in WS PA was the serotonin transporter SERT (*SLC6A4*) (downregulated >60-fold compared to donor PA). A number of other serotonin pathway-related genes were also differentially regulated. Protein kinase C and mitogen-activated protein kinase, which regulate SERT activity, were also downregulated. Serotonin receptor *HTR2A* was increased >3-fold and *MAOB*, the mitochondrial enzyme responsible for metabolizing catecholamines other than serotonin, was upregulated 5-fold. Of note, while *MAOA* was decreased, the expression of *MAOB* was increased.

Protein–protein interaction groups among genes highly regulated in WS PA

We analyzed potential protein–protein interactions among two of the more highly regulated GO groups: ECM and serotonin metabolism (Supplemental Table S2). The results illustrated in Fig. 4 demonstrate a high degree of interaction within the two clusters. Networks of extensive protein interactions are evident, with clusters involving serotonin transport and metabolism, as well as ECM homeostasis mediated by TGFbeta, VWF, and WNT

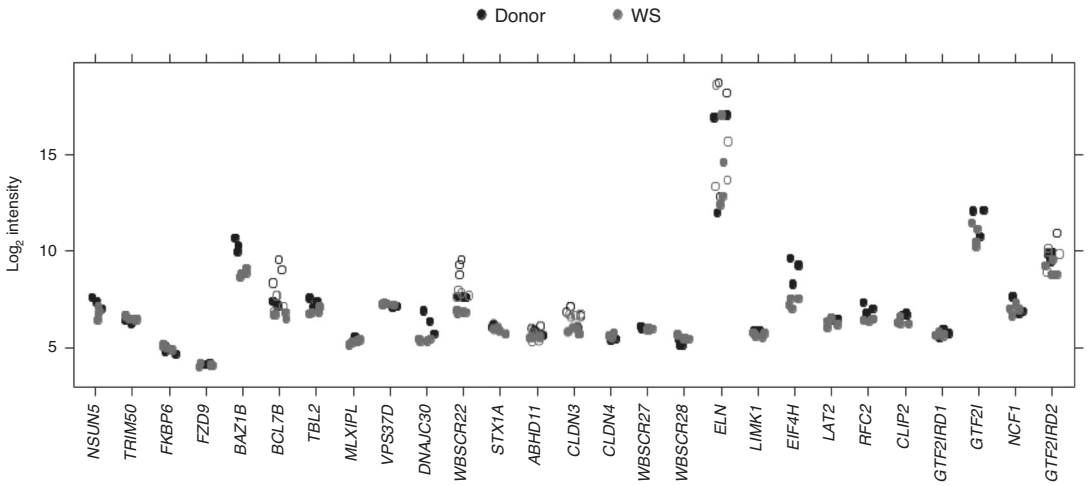

Fig. 3 Expression levels of known genes within the WS-affected region of chromosome 7. Shown are individual expression ($\log_2$ intensity) levels for 32 known WS gene transcripts in all PA samples analyzed in this study. Filled dots, coding transcripts; open circles, noncoding. Red, WS. Black, donor.

Table 4. Signaling pathway genes linked to serotonin transporter.

Gene symbol	Fold change	Description
SLC6A4	−61	Solute carrier family 6 member 4 (serotonin transporter)
HTR2A	3.16	5-Hydroxytryptamine (serotonin) receptor 2A
MAOA	−5.34	Monoamine oxidase A
MAOB	5.73	Monoamine oxidase B
PRKCB	−2.45	Protein kinase C, beta
PRKCD	−2.24	Protein kinase C, delta
MAPK14	−2.02	Mitogen-activated protein kinase 14

receptors and integrins. Further, the two clusters connect through node proteins PER2 and GPX3.

Differences in histological features of WS PA compared to donor PA

PAs from patients with WS exhibit distinct differences from age-matched controls, including an increased arterial wall thickness (i.e., medial hypertrophy), a highly disorganized elastin fiber arrangement, and increased proteoglycan deposition between smooth muscle layers. As shown in Fig. 5, the tunica media was approximately 4-fold thicker in WS PA (1.796 ± 0.298 mm) compared to donor PA (0.388 ± 0.135 mm; ($p < 0.0001$). The medial layer was significantly thicker, and elastin fiber organization was markedly disrupted. The expected characteristic parallel arrangement of elastin fibers between muscle bands was replaced by

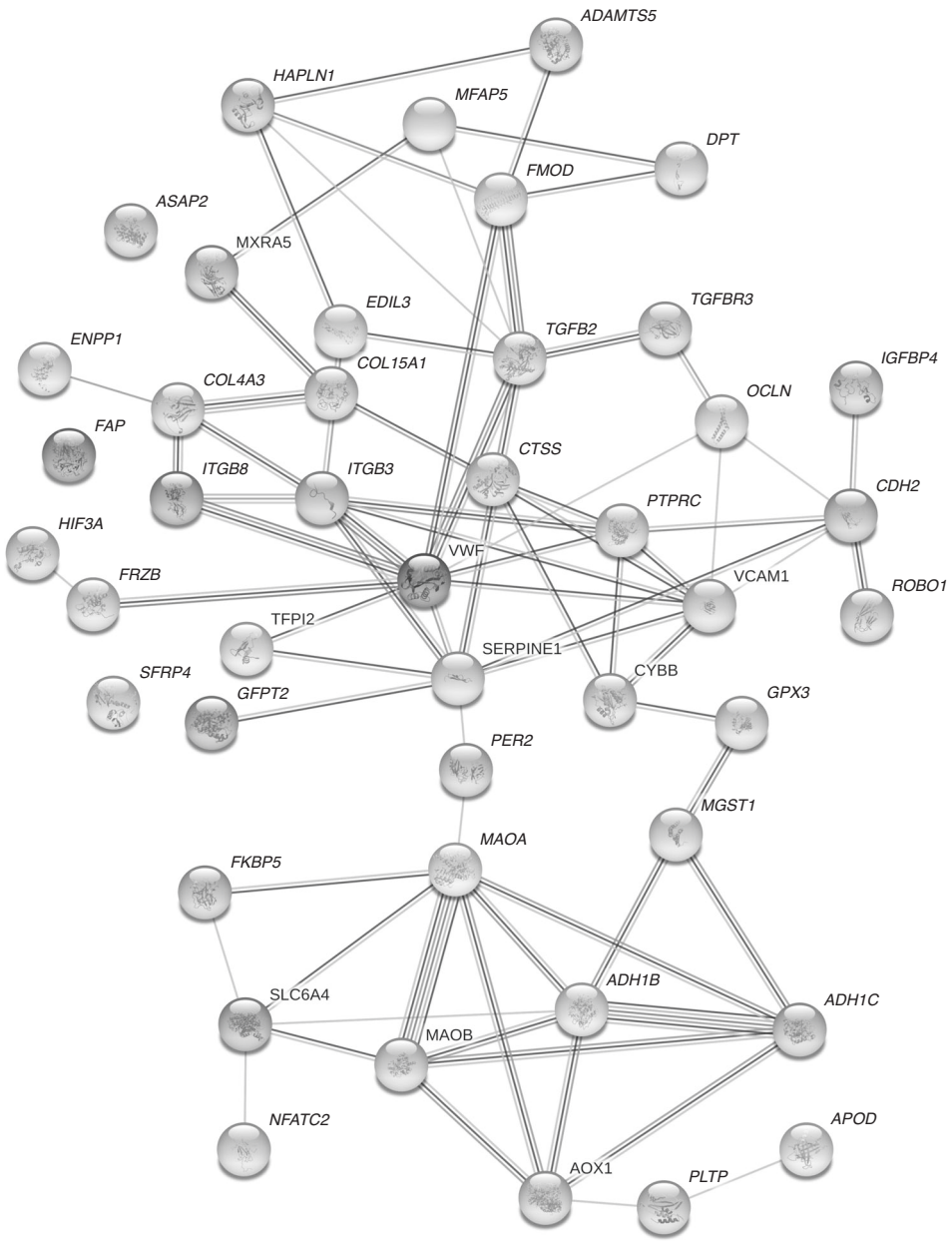

Fig. 4 Protein–protein interaction nodes for differentially regulated genes in the extracellular matrix and serotonin metabolism categories. The diagram illustrates potential interactions among proteins corresponding to genes differentially regulated in WS, based on known interactions curated in the String.org database. Proteins connected by lines are known to interact. The propensity to interact is indicated by line thickness.

randomly dispersed tracts throughout the smooth muscle layer. A prominent proteoglycan-rich matrix was deposited between smooth muscle bands throughout the WS PA medial layer. An apparent increase in spacing between elastic strands was associated with increased proteoglycan content. The density of cells in the WS PA medial layer was similar to donor PA, with an average of 100.8 ± 25.7 cells per high-power field (hpf) in WS and 125.3 ± 28.7 cells per hpf in donor PA; $p = 0.13$.

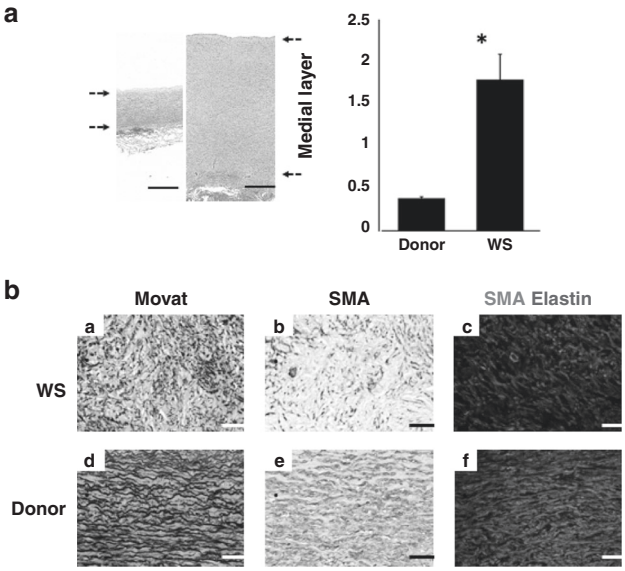

Fig. 5 Cellular architecture difference between WS PA vs donor PA. a H&E staining for donor WS PA shows the difference in medial layer between the two specimens. The medial layer was measured from the base of the sub-endothelium to the adventitia in each sample. The average medial layer width differed >4-fold between donor and Williams syndrome (Donor, 0.388 ± 0.135, $n = 3$; WS, 1.796 ± 0.298, $n = 6$; $*p < 0.0001$; t test). Scale bar = 200 micron. **b** Increased magnification of the tunica media reveals parallel elastic lamellae separated by single layers of smooth muscle cells. Representative serial sections staining for WS PA (top row) and donor PA (bottom row) at ×40 magnification. Movat Pentachrome (left panels a, d) stain includes nuclei (black); fibrin (red); collagen (yellow); proteoglycans/ground substance/mucin (blue); and elastic fibers (black). Disorganization of elastin structure was observed in WS tissue characterized by shorter, non-parallel elastin strands with increased spacing between elastic lamellae. Proteoglycan content was increased in Williams syndrome PA donor PA. IHC staining (middle panels b, e) shows a decrease in the number of SMA-positive cells within the medial layer of WS PA. Immunofluorescent staining (right panels c, f) of elastin (red) and SMA (green) in PA vessel reveals multiple clusters of smooth muscle cells separated by thin, shorter elastic fibers in WS PA. Scale bar = 50 micron.

Co-localization of elastin and smooth muscle alpha-actin
SMA staining demonstrated distinct differences in the distribution and patterning of SMC in WS PA compared to donors (Fig. 5). Whereas WS PA demonstrated disorganized elastic lamellae, donor PA had organized lamellae separated by single layers of SMCs.

Localization of serotonin transporter and receptors
We performed immunolocalization of *SCLC6A* protein product SERT to define the pattern of distribution within PA arterial wall and to examine the association of SERT with receptors. As shown in Fig. 6, SERT staining was evident in the endothelial cell layer as well as in SMCs of donor PA but was minimally expressed in WS PA. We observed that an increased number of serotonin receptor HTR2A stained putative SMCs in WS PA compared with donor PA, while receptor HTR1A showed similar distribution in both the groups.

DISCUSSION

In this study, we sought to analyze the histological, biochemical, and genetic regulatory profiles in samples of PAs from patients with WS and compared them to donor controls as a means of further understanding the development of PPAS in WS. Our study revealed distinct differences in SMC organization in WS PA indicative of medial degeneration and multiple gene regulation differences consistent with medial degenerative processes and an active inflammatory response. Marked changes observed in expression of genes in the serotonin signaling pathway illuminate potential mechanisms by which the development of PPAS in WS may be evoked.

Tunica media structure and cellular morphology in WS PA
Structural differences in WS PA observed in this study include thicker walls, disorganized elastin fibrils, and increased proteoglycan content. These differences are consistent with anecdotal surgeon reports of a more "tough, rubber-like" feel to the vessel than normal PA and with medial degeneration, as described in thoracic aorta disease. Arterial wall degeneration impairs the homeostatic mechanosensing feedback loop in two ways: an excess proteoglycan content increases their shock-absorbing action,[16] reducing sensitivity for force detection,[17] and thereby impairs the elastin–beta catenin–nuclear signal transduction pathway component.[6,18,19] Computational modeling has confirmed a role for proteoglycans in force sensing and that

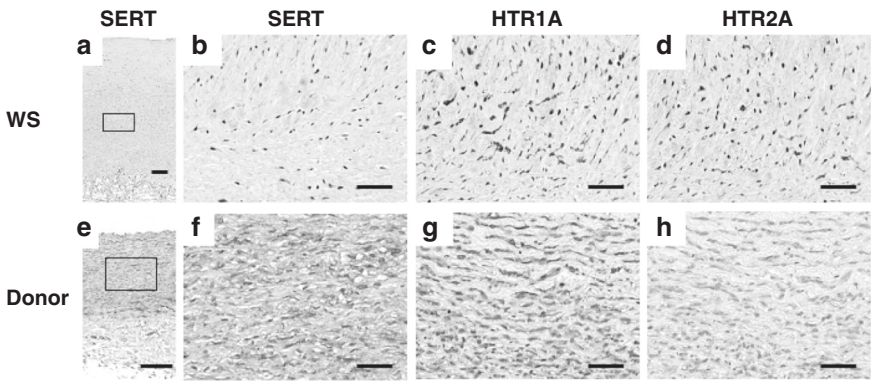

Fig. 6 Expression and localization of SERT and serotonin receptors in human PA. Serial sections of WS PA (**a**–**d**) and donor PA (**e**–**h**) specimens demonstrate immunolocalization of SERT, HTR1A, and HTR2A as indicated by the labeling along the top of the figure. Expression of SERT was observed in the endothelial layer and middle tunica layer of donor PA, whereas the expression of SERT is limited to rare cells in WS PA. Scale bars: **a**, **e**, 200 micron; **b**–**d**, **f**–**h**, 50 micron.

changes in their content modifies force change detection.[20] Of note, loss of the force-shielding effects of proteoglycans due to their degradation is recognized as a key process in aging-related vascular diseases, including aneurysms.[21]

Gene expression profile differences

Comparison of the transcriptomes of WS and donor PAs demonstrated the differential expression of multiple genes. Two aspects of expression changes are of particular interest. First, the observed PA wall structural changes are similar to aortic disease, and genes are regulated in a parallel manner in both arteries. Second, the striking differences in serotonin signaling gene expression indicate the potential for a highly elevated level of extracellular serotonin in WS, a condition that may play a role in the development of PPAS. Chronically increased activation of the serotonin receptor elevates reactive oxygen species (ROS) production, causing unrestricted vasoconstriction and fibrotic changes in the vascular wall.[22] Further, excessive ROS exposure can modify tropoelastin and subsequently alter elastic fiber assembly.[23] WS PA may therefore be more vulnerable to elevated shear stress due to the combined effects of *ELN* haploinsufficiency and serotonin-driven ROS generation, thereby resulting in the severe stenosis manifest as PPAS.

In various arterial disease states, mechanosensing is abnormal. In those states, the expression of several genes responsible for arterial structure and function is altered. ADAMTS5 is a gene known to be abnormally expressed in arterial disease states with impaired mechanosensing. In our study, PA samples from patients with WS exhibited significant changes in the expression of multiple genes associated with mechanosensing, including ADAMTS5, HAPLN1, and MXRA5. Similarly, elastin-contractile units play a key role in mechanosensing in the aorta.[6] Given the changes in elastin lamellar structure seen in not only our study but also in the work of others, these findings suggest strongly that the mechanosensing properties of the arterial wall are impaired in patients with WS and likely are intrinsic to the arterial pathology.

CONCLUSIONS

Although PPAS can develop in association with a variety of other cardiac defects, its prevalence is higher in WS. In this study, we demonstrate gene expression differences that may cause PA in patients with WS to respond abnormally to nonlaminar blood flow at bifurcations. This is conceivably mediated through 5-hydroxytryptamine (5HT)-activated receptors, possibly with the additional influence of ROS within vascular cells. Therefore, we speculate that the altered extracellular architecture and reduced serotonin metabolism in WS PA disrupts biomechanical homeostasis, which, in the presence of elevated flow shear forces, increases the probability of fibrotic changes, thereby fostering PA stenosis at points of highest flow shear. Hence, the WS genotype may enable a phenotype characterized by an extreme response to flow shear early in development that results in profibrotic changes at points of high shear, from which vessels do not recover and their growth potential is altered in regions of disturbed blood flow, culminating in PPAS.

Limitations

Our study is necessarily limited to tissue availability, which is the small amount of tissue discarded during surgical repair operations for PPAS. The technique for repair of PPAS lesions at our institution[8] utilizes the entire region of ostial stenosis. Hence, the tissue used in the studies we report here is limited to that from the main PA, which was discarded during its re-anastomosis. The data we report pertain to analyses of the main PAs of syndromic WS patients and donor controls. Though donor tissue used for controls appeared to be histologically normal and was approved for organ transplant, whether it was completely disease free was not further established. Neither increased tissue 5HT levels in WS PA nor impaired degradation was demonstrated in this study. Until MAO activity is quantified in WS PA, the physiological significance of the reciprocal changes in MAO subtype expression we discovered remain unknown. This study utilized microarrays targeting the entire human transcriptome and mRNA derived from sampling the entire vessel tissue. Future studies examining gene expression at the single-cell level may provide further insight into the unique differences of WS PAs.

ACKNOWLEDGEMENTS

These studies were supported by the congenital division of the department of Cardiothoracic Surgery.

AUTHOR CONTRIBUTIONS

Substantial contributions to conception and design, acquisition of data, or analysis and interpretation of data: all authors. Drafting the article or revising it critically for important intellectual content: X.M., R.T.C., A.G., and R.K.R. Final approval of the version to be published: X.M., R.T.C., and R.K.R.

ADDITIONAL INFORMATION

The online version of this article (https://doi.org/10.1038/s41390-020-01359-5) contains supplementary material, which is available to authorized users.

Competing interests: The authors declare no competing interests.

Patient consent: Human specimen collection was conducted under a Stanford University-approved expedited IRB protocol in which patient consent was not required.

Publisher's note Springer Nature remains neutral with regard to jurisdictional claims in published maps and institutional affiliations.

REFERENCES

1. Pober, B. R. Williams-Beuren syndrome. *N. Engl. J. Med.* **362**, 239–252 (2010).
2. Adams, G. N. & Schmaier, A. H. The Williams-Beuren Syndrome-a window into genetic variants leading to the development of cardiovascular disease. *PLoS Genet.* **8**, e1002479 (2012).
3. Angelov, S. N., Zhu, J., Hu, J. H. & Dichek, D. A. What's the skinny on elastin deficiency and supravalvular aortic stenosis? *Arterioscler. Thromb. Vasc. Biol.* **37**, 740–742 (2017).
4. Collins, R. T. 2nd, Kaplan, P., Somes, G. W. & Rome, J. J. Cardiovascular abnormalities, interventions, and long-term outcomes in infantile Williams syndrome. *J. Pediatr.* **156**, 253–258.e251 (2010).
5. Collins, R. T. 2nd, Kaplan, P., Somes, G. W. & Rome, J. J. Long-term outcomes of patients with cardiovascular abnormalities and williams syndrome. *Am. J. Cardiol.* **105**, 874–878 (2010).
6. Karimi, A. & Milewicz, D. M. Structure of the elastin-contractile units in the thoracic aorta and how genes that cause thoracic aortic aneurysms and dissections disrupt this structure. *Can. J. Cardiol.* **32**, 26–34 (2016).
7. Li, D. Y. et al. Elastin is an essential determinant of arterial morphogenesis. *Nature* **393**, 276–280 (1998).
8. Martin, E., Mainwaring, R. D., Collins, R. T. 2nd, MacMillen, K. L. & Hanley, F. L. Surgical repair of peripheral pulmonary artery stenosis in patients without Williams or Alagille syndromes. *Semin. Thorac. Cardiovasc. Surg.* **32**, 973–979 (2020).
9. Jiao, Y. et al. Deficient circumferential growth is the primary determinant of aortic obstruction attributable to partial elastin deficiency. *Arterioscler. Thromb. Vasc. Biol.* **37**, 930–941 (2017).
10. Li, D. Y. et al. Novel arterial pathology in mice and humans hemizygous for elastin. *J. Clin. Investig.* **102**, 1783–1787 (1998).
11. Mochizuki, S., Brassart, B. & Hinek, A. Signaling pathways transduced through the elastin receptor facilitate proliferation of arterial smooth muscle cells. *J. Biol. Chem.* **277**, 44854–44863 (2002).
12. Parrish, P. C. R. et al. Whole exome sequencing in patients with Williams-Beuren syndrome followed by disease modeling in mice points to four novel pathways that may modify stenosis risk. *Hum. Mol. Genet.* **29**, 2035–2050 (2020).
13. Collins, R. T. 2nd Cardiovascular disease in Williams syndrome. *Circulation* **127**, 2125–2134 (2013).

14. Monge, M. C. et al. Surgical reconstruction of peripheral pulmonary artery stenosis in Williams and Alagille syndromes. *J. Thorac. Cardiovasc. Surg.* **145**, 476–481 (2013).
15. Ma, X. et al. Tetralogy of Fallot: aorto-pulmonary collaterals and pulmonary arteries have distinctly different transcriptomes. *Pediatr. Res.* **76**, 341–346 (2014).
16. Shen, Y. H., Lu, H. S., LeMaire, S. A. & Daugherty, A. Unfolding the story of proteoglycan accumulation in thoracic aortic aneurysm and dissection. *Arterioscler. Thromb. Vasc. Biol.* **39**, 1899–1901 (2019).
17. Milewicz, D. M. et al. Altered smooth muscle cell force generation as a driver of thoracic aortic aneurysms and dissections. *Arterioscler. Thromb. Vasc. Biol.* **37**, 26–34 (2017).
18. Ingber, D. E. Tensegrity-based mechanosensing from macro to micro. *Prog. Biophys. Mol. Biol.* **97**, 163–179 (2008).
19. Wang, N., Tytell, J. D. & Ingber, D. E. Mechanotransduction at a distance: mechanically coupling the extracellular matrix with the nucleus. *Nat. Rev. Mol. Cell Biol.* **10**, 75–82 (2009).
20. Roccabianca, S., Bellini, C. & Humphrey, J. D. Computational modelling suggests good, bad and ugly roles of glycosaminoglycans in arterial wall mechanics and mechanobiology. *J. R. Soc. Interface* **11**, 20140397 (2014).
21. Humphrey, J. D., Milewicz, D. M., Tellides, G. & Schwartz, M. A. Cell biology. Dysfunctional mechanosensing aneuryms. *Science.* **344**, 477–479 (2014).
22. Pena-Silva, R. A., Miller, J. D., Chu, Y. & Heistad, D. D. Serotonin produces monoamine oxidase-dependent oxidative stress in human heart valves. *Am. J. Physiol. Heart Circ. Physiol.* **297**, H1354–H1360 (2009).
23. Akhtar, K. et al. Oxidative and nitrosative modifications of tropoelastin prevent elastic fiber assembly in vitro. *J. Biol. Chem.* **285**, 37396–37404 (2010).